ECCOMAS Congress 2016
VII European Congress on Computational Methods in Applied Sciences and Engineering
M. Papadrakakis, V. Papadopoulos, G. Stefanou, V. Plevris (eds.)
Crete Island, Greece, 5–10 June 2016

CONVERGENCE ANALYSIS OF STRESS FIELDS TO HOMOGENIZATION PREDICTIONS IN OPTIMAL PERIODIC COMPOSITE DESIGN

Pedro G. Coelho[1], Rui A. Reis[1], and José M. Guedes[2]

[1] UNIDEMI, DEMI, FCT-UNL
2829-516 Caparica
{pgc@fct.unl.pt, rf.alvesreis@gmail.com}

[2] IDMEC, Instituto Superior Técnico, Universidade de Lisboa
1049-001 Lisboa
jmguedes@tecnico.ulisboa.pt

Keywords: Homogenization, Composites, Cellular, Stress, Topology, Optimization.

Abstract. *Homogenization assumes that a unit-cell of a periodic composite material is infinitely small and it has periodic boundary conditions. In practice, such material comprises a finite number of measurable unit-cells and the stress fields are not periodic near the structure boundary. It is thus critical to investigate in the scope of the present work whether the optimized unit-cell topologies obtained are affected when applied in the context of real composites. This is done here by scaling the unit-cell an increasing number of times and accessing the micro (or local) stresses of the resulting composite by means of standard numerical experiments and comparing them to the homogenization predictions. The outcome indicates that it is sufficient to have a low scale factor to replace the non-homogeneous composite by the equivalent homogeneous material with the stress field computed by homogenization.*

1 INTRODUCTION

Stress-based topology optimization problems are more realistic to engineering practice than the conventional maximum stiffness approaches because one may guarantee not only very efficient designs but also feasible ones. However, dealing with stress criteria is specially challenging due to the: (1) "singularity" problem; (2) local nature of the stress constraint; (3) highly non-linear stress behavior. Several contributions have been made to handle these issues to the point that fine results are now obtained for macroscopic structures [1-4]. The present paper expands the analysis of stresses to material microstructures which may lay the groundwork for the optimal topology design of material "unit-cells" including stress criteria [5]. An "unit-cell" represents here the smallest periodic heterogeneity of periodic composite/cellular media. In general, periodic homogenization models are used to compute the elastic properties and local stresses of periodic composite materials based on the shape/periodicity of a given material unit-cell [6,7]. Conversely, in material design, the unit-cell is not known a priori, and the goal is to design it to attain specific properties values – inverse homogenization problem [8]. This design problem is solved here by formulating it as an optimization problem. However, homogenization assumes that the unit-cell is infinitely small and it has periodic boundary conditions (BC's). In practice, the composite material comprises a finite number of measurable unit-cells and the stress fields are not periodic near the structure boundary. It is thus critical to investigate in the scope of the present work whether the obtained unit-cell topologies are affected when applied in the context of real composites. This is done here by scaling the unit-cell an increasing number of times and accessing the micro (or local) stresses of the resulting composite by means of standard numerical experiments and comparing them to the homogenization predictions. This furthers previous work [9] related to compliance and elastic coefficients convergence to homogenization predictions. Here, the outcome also indicates that it is sufficient to have a low scale factor to replace the non-homogeneous composite by the equivalent homogeneous material with the stress field computed by homogenization.

2 MATERIAL MODEL

Figure 1 presents the periodic material model mixing strong, $E^{(1)}$, and weak, $E^{(2)}$, materials (see also [9]). The unit-cell volume Y (of feature size d) is cubic and one repeats it n^3 times resulting in volume Ψ ($D = |\Psi| = 1$). Therefore, the ratio $n = D/d$ can be seen as a scale factor.

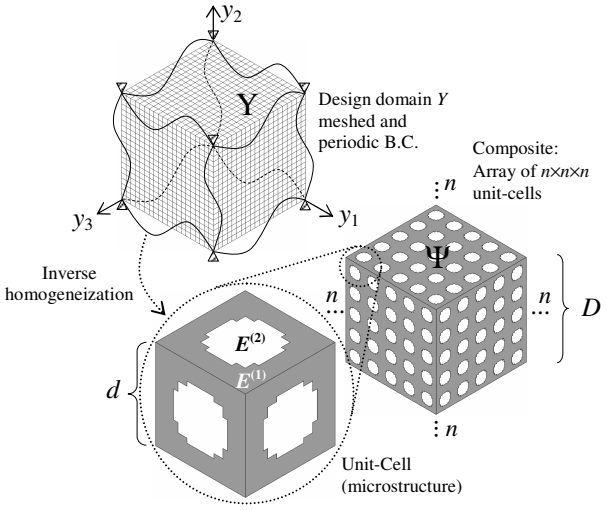

Figure 1: Material model. Finite element discretization of Y with periodic BC's. Array of 5×5×5 unit-cells of global size D (macroscale) and one unit-cell of size d (microscale).

The asymptotic homogenization model used implies that stresses are calculated when $n \to \infty$ and thus no size is given to the unit-cell, i.e. $d \to 0$. The stiffness ratio, $E^{(1)}/E^{(2)}$, is here equal to 10^1 or 10^{12} representing a composite or cellular material, respectively. Both phases are solid isotropic. One keeps phase 1 as the reference, i.e. $E^{(1)} = 300\text{MPa}$ and $\nu = 0.3$ (properties of a biodegradable polymer currently used in scaffolds for tissue engineering, see [10]).

3 OPTIMIZATION PROBLEM

The unit-cell topology shown in Figure 2 is obtained by inverse homogenization solving the following compliance minimization problem subject to a volume fraction constraint [11],

$$\min_{\boldsymbol{\mu}} \quad \frac{1}{2}\boldsymbol{\sigma}^0 \mathbf{C}^{\mathrm{H}}(\boldsymbol{\mu})\boldsymbol{\sigma}^0 \qquad \text{s.t.} \quad \int_Y \mu(\mathbf{y})\,\mathrm{d}Y \le V^* \tag{1}$$

Here $\boldsymbol{\sigma}^0$ is a macroscopic hydrostatic stress state ($\sigma = 1\text{MPa}$), volume $|\mathrm{Y}| = 1$ and $\mathbf{C}^{\mathrm{H}}$ is the homogenized compliance tensor computed as the inverse of the stiffness tensor $\mathbf{E}^{\mathrm{H}}$ through,

$$E^{\mathrm{H}}_{ijmn}(\mu) C^{\mathrm{H}}_{mnkl}(\mu) = \frac{1}{2}\left(\delta_{ik}\delta_{jl} + \delta_{il}\delta_{jk}\right) \tag{2}$$

where δ_{ij} are Kronecker deltas and,

$$E^{\mathrm{H}}_{ijkm}(\mu) = \frac{1}{|\mathrm{Y}|}\int_{\mathrm{Y}} E_{pqrs}(\mu)\left(\delta_{pk}\delta_{qm} - \frac{\partial \chi^{km}_p}{\delta y_q}\right)\left(\delta_{ri}\delta_{sj} - \frac{\partial \chi^{ij}_r}{\delta y_s}\right)\mathrm{dY} \tag{3}$$

with the microstructure material elastic properties, E_{pqrs}, depending on density design variables, $\boldsymbol{\mu}$, in order to interpolate between two base materials according to the power law,

$$E_{pqrs}(\mu) = \mu^p E^{(1)}_{pqrs} + \left(1 - \mu^p\right)E^{(2)}_{pqrs}, \quad p \in \mathbf{N} \tag{4}$$

and the homogenized tensor depends on the material unit cell deformation modes or micro-displacements χ^{kl} (Y-periodic), which are solution of the set of equilibrium equations defined in Y (six equations in three dimensions),

$$\int_{\mathrm{Y}} E_{ijpq}(\mu)\frac{\partial \chi^{kl}_p}{y_q}\frac{\partial w_i}{\partial y_j}\mathrm{d\,Y} = \int_{\mathrm{Y}} E_{ijkl}(\mu)\frac{\partial w_i}{\partial y_j}\mathrm{d\,Y}, \quad \forall_w \ \mathrm{Y-periodic} \tag{5}$$

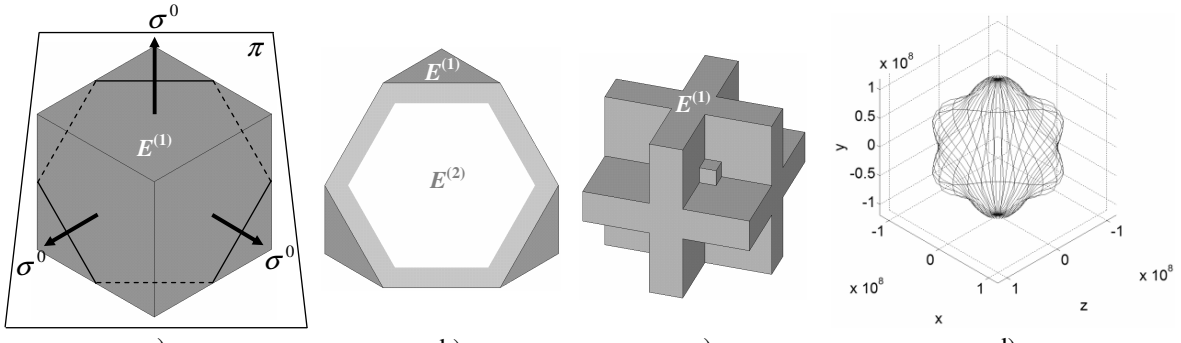

a) b) c) d)

Figure 2: Unit-cell. a) Box-type (isometric view); b) Section view using cutting plane π normal to the octahedral direction, c) Shifted design results from translation along octahedral direction (material 2 is unselected only for design comprehension, see also [10]); d) Graphical representation of anisotropy as in [9], units in [Pa].

4 STRESS ANALYSIS

4.1 Homogenization prediction

The micro-stresses σ_{ij} (in the level of material microstructure) are obtained from asymptotic homogenization theory, by considering the displacement test fields χ_k^{rs} from Eq. (5) as,

$$\sigma_{ij} = E_{ijkm}\left(\delta_{kr}\delta_{ms} - \frac{\partial \chi_k^{rs}}{\partial y_m}\right)\varepsilon_{rs}^0 \tag{6}$$

where ε_{rs}^0 is the macroscopic (average) strain field related to the macroscopic stress in (1),

$$\varepsilon_{rs}^0 = C_{rspq}^H \sigma_{pq}^0 \tag{7}$$

The σ_{ij} results represent the three-dimensional stress states varying throughout the unit-cell domain Y (see Figure 4a). Here, the methodology used for obtaining such stresses is based on the software POSTMAT [12,13].

4.2 Numerical experiments

The commercial finite element code ANSYS@ is used here to perform standard numerical testing procedures with specific BC's to calculate the stress field inside the domain Ψ of the periodic composite/cellular material as the scale factor *n* increases from 1 to 5, see periodic patterns in Figure 3. It is shown half the domain, $|\Psi|/2$, in order to highlight the central unit-cell where the stress field is measured (see also Figure 4b,c) and compared to the results given by homogenization running POSTMAT (Figure 4a). Shifted design (as shown in Figure 2c) must be used in some arrays (for *n* = even number) to guarantee that the unit-cell topology extracted from the center of the periodic pattern matches exactly the one (no-shifted) evaluated by POSTMAT. Finite element meshes for each periodic pattern are not shown in Figure 3 because they would become so refined with increasing *n* that elements wouldn't be clearly observed. Anyway, each unit-cell comprises a regular mesh 10×10×10 of 8-node isoparametric hexahedral finite elements. This means that a total of $1000\times n^3$ finite elements are used in the numerical model associated with scale factor *n*.

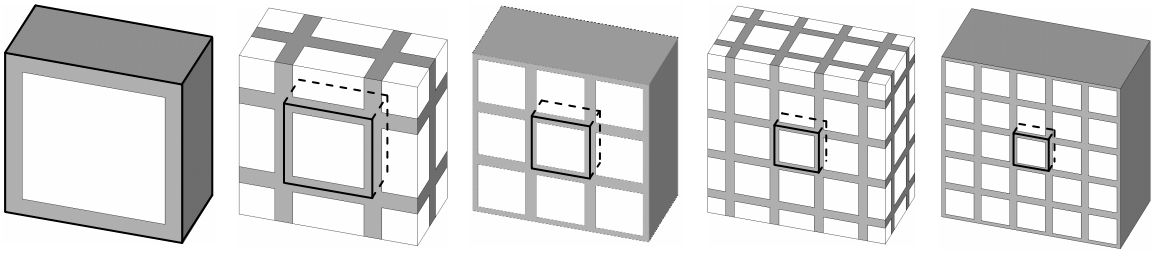

1×1×1 2×2×2 3×3×3 4×4×4 5×5×5

Figure 3: Volume Ψ (half represented) containing arrays *n*×*n*×*n* of unit-cells where *n* varies from 1 to 5. Unit-cell design is shifted when arrays take even numbers. The unit-cell located at the center of Ψ is highlighted.

One considers the Dirichlet and Neumman-type BC's (see [9,14]) given by, respectively,

$$\mathbf{u}(\mathbf{y})\big|_{\partial\Psi} = \boldsymbol{\Theta}\cdot\mathbf{y}\big|_{\partial\Psi} \tag{8}$$

$$\boldsymbol{\sigma}^0(\mathbf{y})\cdot\mathbf{n}\big|_{\partial\Psi} = \boldsymbol{\Theta}\cdot\mathbf{n}\big|_{\partial\Psi} \tag{9}$$

$$\text{where } \boldsymbol{\Theta} = \begin{bmatrix} \beta & 0 & 0 \\ 0 & \beta & 0 \\ 0 & 0 & \beta \end{bmatrix} \tag{10}$$

and $\partial\Psi$ is the boundary of Ψ, **u** is the displacement vector, **y** is the spatial position vector, **n** is the outward normal unit vector and β is the constant characterizing the hydrostatic tensor $\boldsymbol{\Theta}$. On one hand, Eq. (8) applies in $\partial\Psi$ a displacement field **y** linearly dependent such that Ψ is tested at a uniform macroscopic strain β, i.e.

$$\varepsilon_{ij}^{0} = \frac{1}{2}\left(\frac{\partial u_i}{\partial y_j} + \frac{\partial u_j}{\partial y_i}\right) = \beta\delta_{ij} \text{ in } \partial\Psi \text{ and on average } \left\langle \varepsilon \right\rangle_{\Psi} = \frac{\int_{\Psi} \varepsilon \, \mathrm{d}\Psi}{|\Psi|} = \beta\delta_{ij} \tag{11}$$

On the other hand, Eq. (9) means that the test is carried out on Ψ at a uniform macroscopic stress β (also on average holds $\left\langle \sigma \right\rangle_{\Psi} = \beta$). In both tests β must be chosen such that consistency with POSTMAT is ensured, see Eq. (6) and (7). However, BC's in Eq. (9) can't be applied to the analysis of cellular (or porous) material, $E^{(1)}/E^{(2)} = 10^{12}$, because the pressure on the top of the finite elements modeling the void phase results in excessive compliance. Nevertheless, Dirichlet-type BC's can be applied to both ratios, 10^{1} (composite) and 10^{12} (cellular).

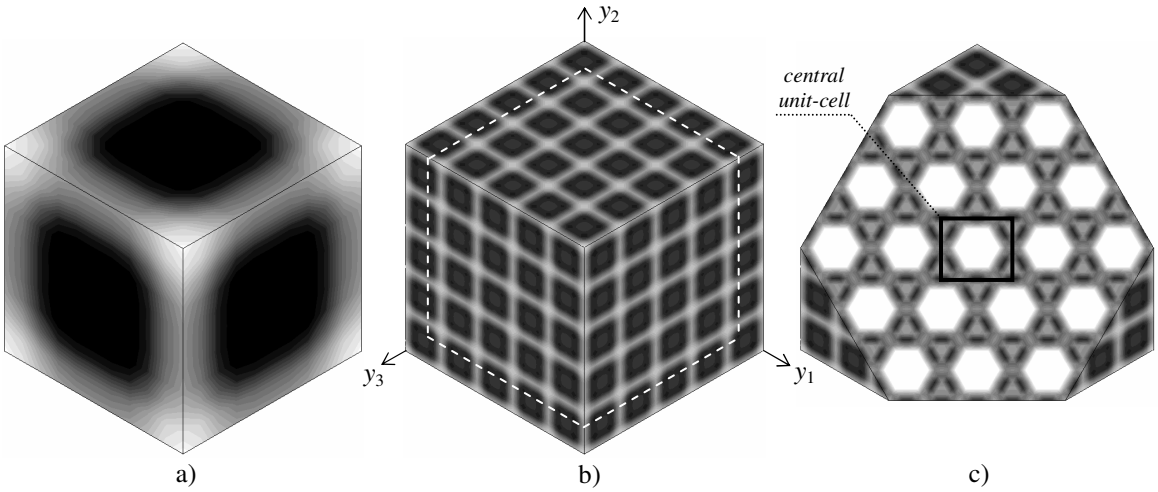

Figure 4: Von-Mises stress is shown for the ratio $E^{(1)}/E^{(2)} = 10^{12}$ (averaged values are shown only for the sake of getting a smoother display). a) POSTMAT results; b) ANSYS results for the array 5×5×5 of unit-cells (undeformed design in dashed lines); c) Section view of the array using plane π as used in Figure 2.

5 CONVERGENCE ANALYSIS

The purpose of this study is the convergence analysis of stress fields to homogenization predictions. These predictions are obtained running the POSTMAT code. Then a battery of ANSYS analyses is carried out such that stresses can be read from the post-processor for each array presented in Figure 3 with specific BC's and stiffness ratio.

ANSYS code provides individual stress components as well as the equivalent stress (Von-Mises) at each node and element. To simplify the comparative analysis between POSTMAT and ANSYS one chooses to compare element equivalent stresses that in ANSYS are computed as follows,

$$\sigma_{eq} = \sqrt{\frac{1}{2}\left[\left(\overline{\sigma}_{11} - \overline{\sigma}_{22}\right)^2 + \left(\overline{\sigma}_{22} - \overline{\sigma}_{33}\right)^2 + \left(\overline{\sigma}_{33} - \overline{\sigma}_{11}\right)^2\right] + 3\left(\overline{\sigma}_{12}^2 + \overline{\sigma}_{23}^2 + \overline{\sigma}_{13}^2\right)} \tag{12}$$

where

$$\overline{\sigma}_{ij} = \frac{\sum_{k=1}^{N} \sigma_{ij}^{k}}{N} \text{ with } N = 8 \text{ (number of Gauss points)} \tag{13}$$

POSTMAT post-processor is properly adapted to do these same calculations of equivalent stress. Finally, one proceeds evaluating the deviation of ANSYS stress results toward POSTMAT according to the formula,

$$\text{Deviation}\,[\%] = \frac{\left(\sigma_{\text{eq}}^{\text{ANSYS}} - \sigma_{\text{eq}}^{\text{POSTMAT}}\right)}{\sigma_{\text{eq}}^{\text{POSTMAT}}} \times 100 \tag{14}$$

This stress deviation measure is evaluated at each finite element of the unit-cell (in the ANSYS model is the central unit-cell, see also Figure 3). Using the mesh 10×10×10, the resulting data for plotting comprises 1000 points. However, due to the symmetry seen in the resulting distribution only half the points are of interest. Therefore, the first five charts presented in Figures 5 to 7 show the elements number (1 to 500) in the abscissa axis and the deviation is represented along the ordinate axis [%]. Each one of these charts is obtained for an increasing number of the scale factor *n*, 1 to 5. Looking only at clusters of points here doesn't help much drawing some conclusions. So, the last chart shown in Figures 5 to 7 is an attempt to provide the scale-size effect analysis in a nutshell and should be seen along with Table 1. This table presents some statistical analysis of the plotted deviations in terms of maximum and minimum values, mean (simple average) and standard deviation. Table 1 and Figures 5 to 7 present data in the same order, i.e. first the composite material case ($E^{(1)}/E^{(2)} = 10^{1}$) is treated and the results with Neumann-type BC's precede the Dirichlet's results. Finally, the cellular material case ($E^{(1)}/E^{(2)} = 10^{12}$) is presented with the respective results considering Dirichlet-type BC's only (as explained in section 4.2).

B.C.	ratio	Measures	1×1×1	2×2×2	3×3×3	4×4×4	5×5×5
Neumann	10^{1}	*max*	3445,707	747,230	70,011	10,301	2,872
		$\overline{e}$	**647,289**	**156,114**	**11,965**	**0,659**	**-0,836**
		min	-47,988	-28,788	-28,786	-5,818	-1,665
		s	**930,933**	**215,734**	**20,560**	**3,174**	**0,540**
Dirichlet	10^{1}	*max*	209,803	21,159	2,770	1,413	1,282
		$\overline{e}$	**2,994**	**-6,564**	**-0,421**	**0,805**	**0,389**
		min	-50,748	-44,030	-5,102	-0,391	-0,226
		s	**32,650**	**12,517**	**1,474**	**0,274**	**0,196**
	10^{12}	*max*	178,462	4,407	1,154	1,536	0,701
		$\overline{e}$	**3,697**	**2,846**	**1,072**	**1,504**	**0,675**
		min	-18,911	-6,465	0,581	1,314	0,656
		s	**30,799**	**1,351**	**0,073**	**0,026**	**0,009**

Table 1: Statistical summary of deviations plotted in Figures 5 to 7. Mean $\overline{e}$, standard deviation **s** and extreme deviations (*max* and *min*) attained [%].

One discusses first the composite stress results in Figures 5 and 6. Here one makes the distinction between the stress deviations measured in the material 1 which is stronger (see the black dots plotted) and material 2 which is weaker (see the empty dots plotted). As a result of separating things this way one concludes that the higher deviations are typically identified with the elements where stress values are lower (material 2), see Figures 5a,b,c and 6a,b,c. In regions where stress values are higher or critical (material 1) the stress values from ANSYS and POSTMAT compare much better which is, in practice, a significant result because ulti-

mately one would compare the maximum value of POSTMAT with the material Yield Stress (σ_Y) for design feasibility. The relative importance of the composite phases in the magnitude of the deviations is far more noticed for low scale factors n, typically between 1 and 3. For $n \geq 4$ the deviations measured in materials 2 become eventually as big as the deviations seen in material 1 and typically both come to be below 2% which is here an excellent convergence result (see Figures 5e and 6e).

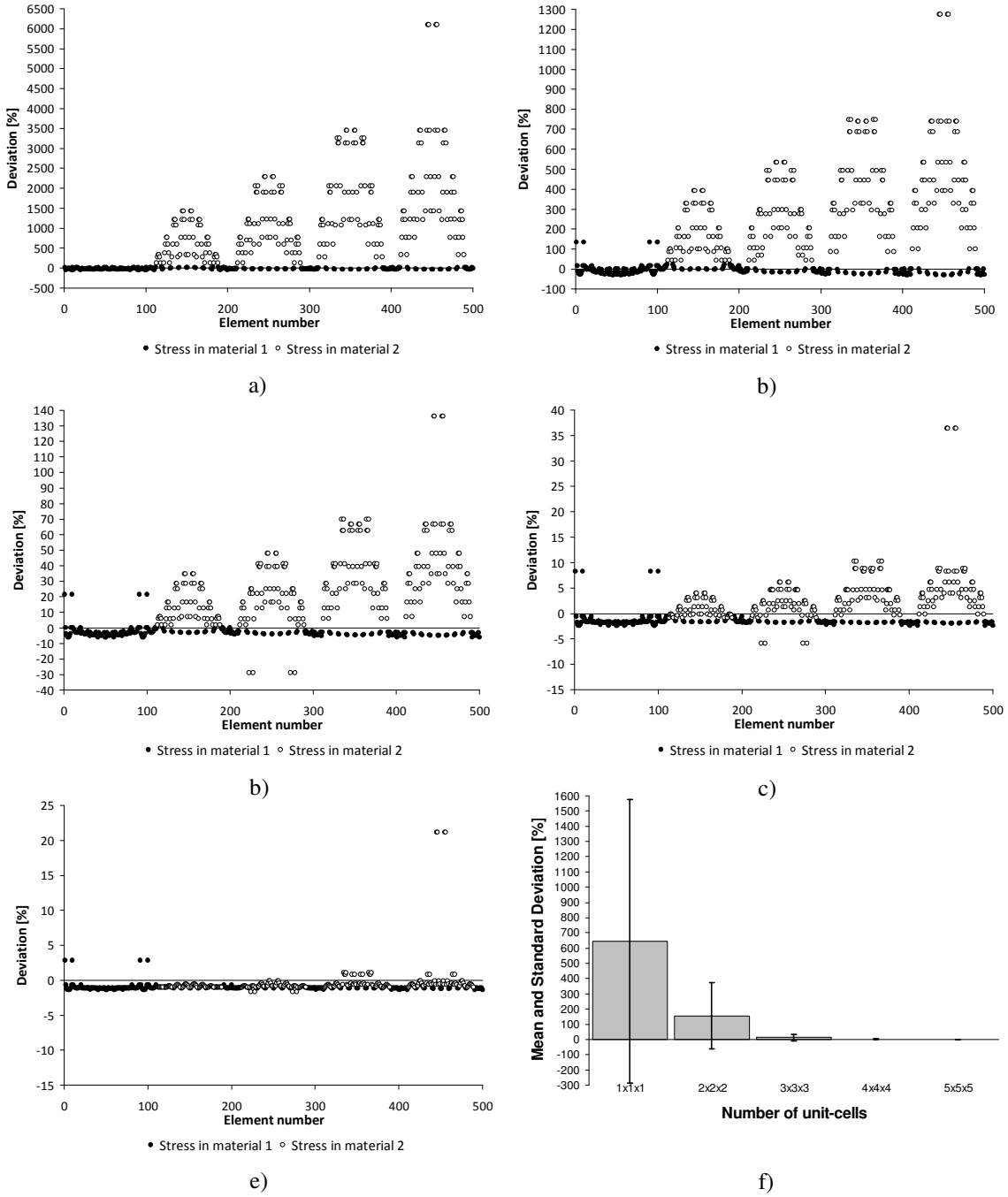

Figure 5: Scale-size effects analysis for **composite $E^{(1)}/E^{(2)} = 10^1$** with **Neumann B.C.** Deviation computed through Eq. (14) in all elements of the central unit-cell taken from different arrays: a) 1×1×1; b) 2×2×2; c) 3×3×3; d) 4×4×4; e) 5×5×5. f) Statistical summary in terms of mean and standard deviation.

However, despite higher *n*, one observes that deviations computed in only four elements (numbers 445, 446, 455, 456) are comparatively much higher, reaching 22%. These elements are located right in the middle of the unit-cell domain Y (in material 2) and their stress value (order of 10^2) is the minimum found in Y whether by POSTMAT or ANSYS (the order of the maximum stress found is 10^6). These deviations are classified here as outliers and the statistical analysis carried out in Table 1 excludes them.

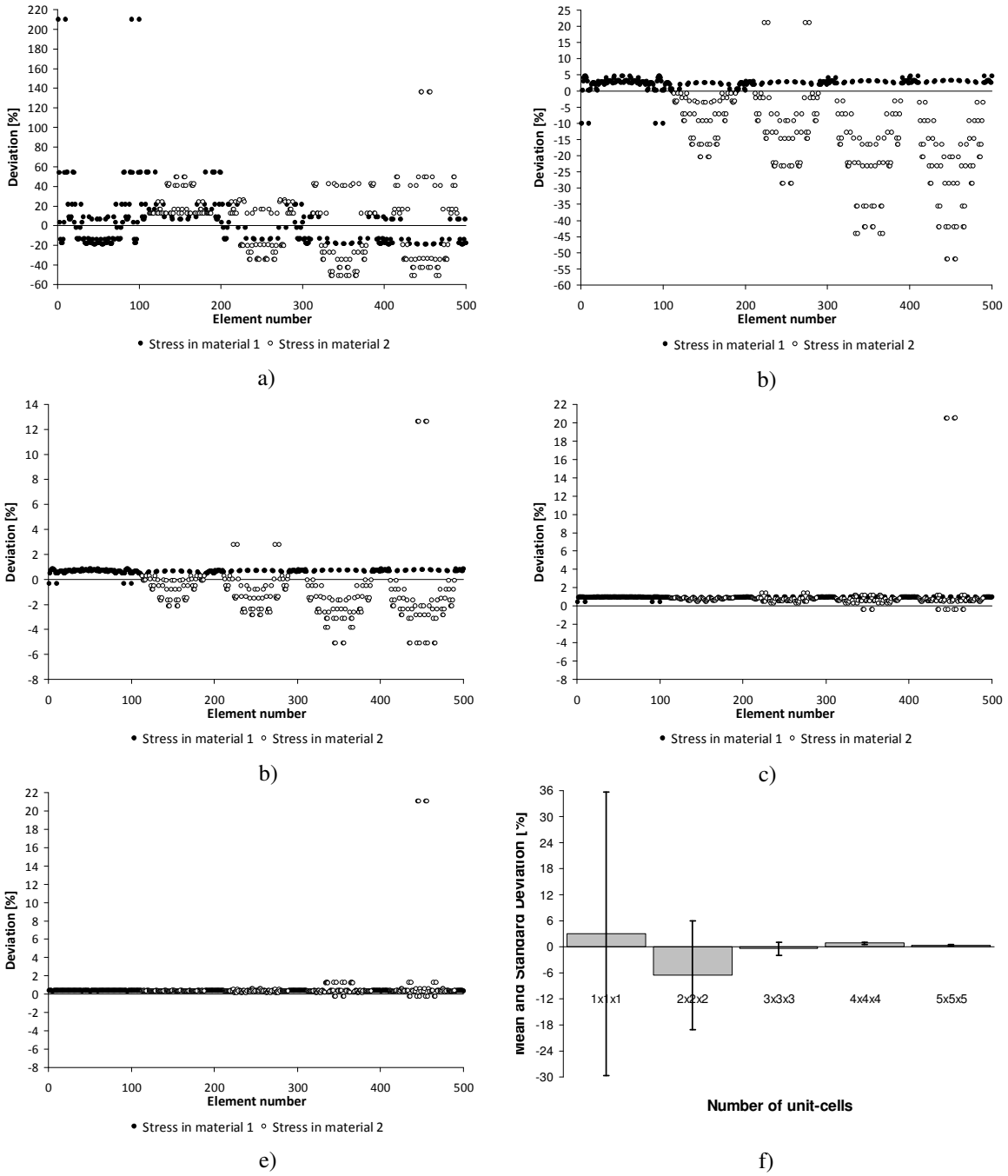

Figure 6: Scale-size effects analysis for **composite $E^{(1)}/E^{(2)} = 10^1$** with **Dirichlet B.C.** Deviation computed through Eq. (14) in all elements of the central unit-cell taken from different arrays: a) 1×1×1; b) 2×2×2; c) 3×3×3; d) 4×4×4; e) 5×5×5. f) Statistical summary in terms of mean and standard deviation.

Considering now the cellular material case, one notices that the stresses are basically zero (e.g. 10^{-6}) in elements representing the void phase that's why one decides overlooking them when calculating deviations and doing statistics (Figure 7 contains then comparatively lesser points). Due to this simplification one notices the standard deviation decreasing faster than the other cases. The *min*, *max* and mean values in Table 1 are all below 1% for $n = 5$ which is impressive for such a low scale factor.

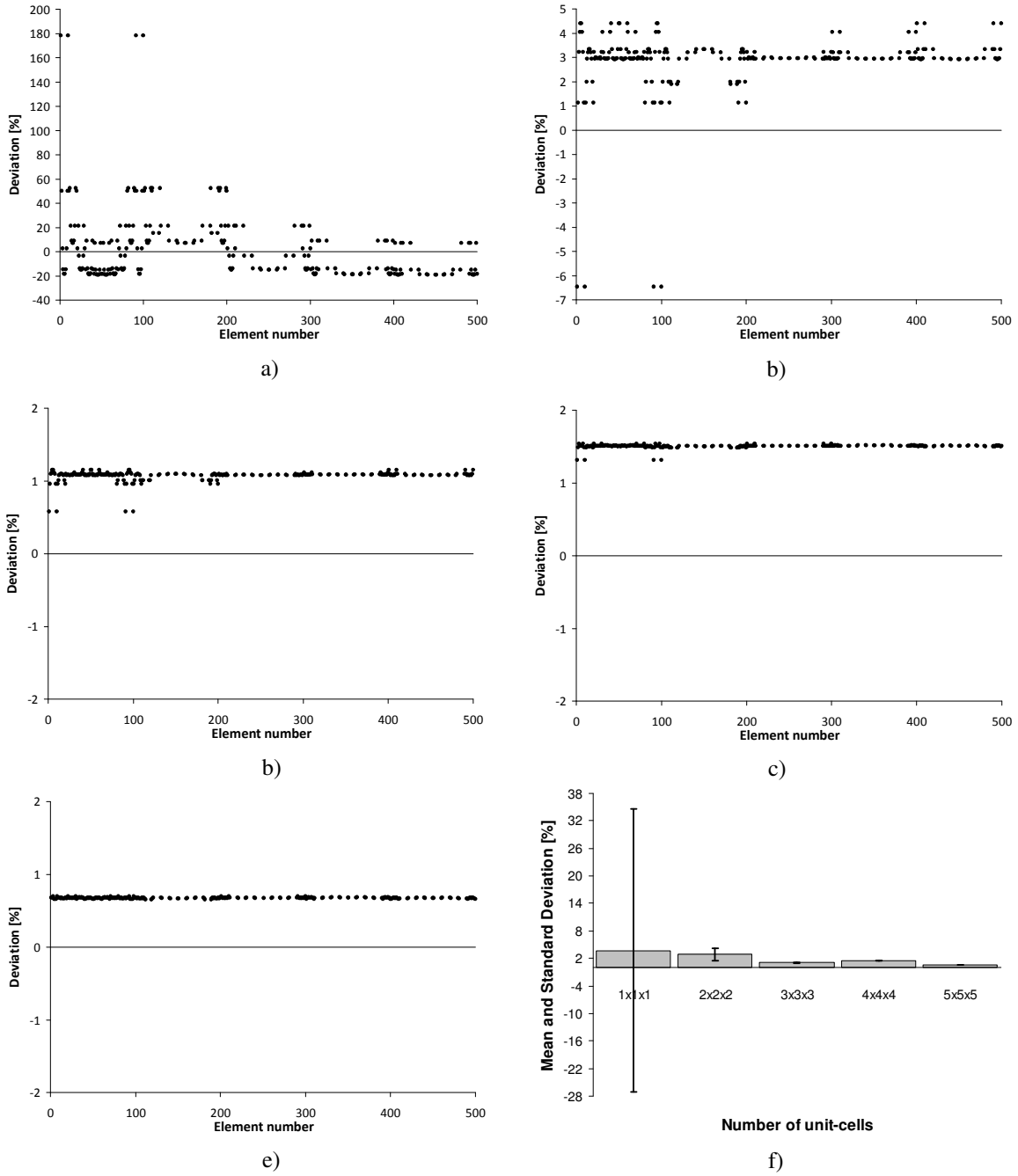

Figure 7: Scale-size effects analysis for **cellular material $\mathbf{E^{(1)}/E^{(2)} = 10^{12}}$** with **Dirichlet B.C.** Deviation computed through Eq. (14) in all elements of the central unit-cell taken from different arrays: a) 1×1×1; b) 2×2×2; c) 3×3×3; d) 4×4×4; e) 5×5×5. f) Statistical summary in terms of mean and standard deviation.

In general, one perceives a fair convergence to the homogenizations predictions. Since the shifted design is used in arrays with even number of unit-cells, it is more fair to compare results among n=1,3,5 and then between n=2,4 because the material distribution in the boundary, $\partial\Psi$, where loads are applied, differs depending on whether the design is shifted or not (see Figure 3). The standard deviation measure gives probably more insight in this analysis than the mean value. The mean may go up and down (changing sign as well) as n increases because ANSYS may target POSTMAT either from above or below. The resulting trend for the mean is not so consistent when compared to the standard deviation trend which always decrease with increasing n. Anyway, for n=5 the mean deviation is below 1% in all cases. The maximum and minimum deviation values are also quite good as a result of excluding outliers as aforementioned.

6 CONCLUSIONS

- Stress-based topology optimization is quite appealing for engineering practice due to the fact that an optimal design must be a feasible one too.
- The inverse homogenization method is straightforward to generate unit-cell designs for periodic composites. However the assumptions of ideal periodicity as well as dimensionless unit-cell have to be checked in the context of real composites which motivates the scale-size effect analysis presented in this work.
- As an outcome the present study indicates that it is sufficient to have a low scale factor (n=5) to replace the non-homogeneous composite by the equivalent homogeneous material with the stress field computed by homogenization.
- A single unit-cell topology design was investigated in this work and a coarse finite element mesh was used to discretize the stress field that is in general highly non-linear. These simplifications may motivate further detailed analyses on scale-size effects.

REFERENCES

[1] J.D. Deaton. R.V. Grandhi. A survey and multidisciplinary continuum topology optimization: post 2000. *Struct Multidisc Optim*. **49**. 1-38. 2014.

[2] M.P. Bendsøe. O. Sigmund. *Topology Optimization: Theory, Methods and Applications.* Springer. 2004.

[3] P. Duysinx. M.P. Bendsøe. Topology optimization of continuum structures with local stress constraints. *Int Journal for Numerical Methods in Engineering*. **43**. 1453-1478. 1998.

[4] M. Bruggi. On an alternative approach to stress constraints relaxation in topology optimization. *Struct Multidisc Optim*. **36**. 125-141. 2008.

[5] R. Lipton. M. Stuebner. Optimization of composite structures subject to local stress constraints. *Computer Methods in Applied Mechanics and Engineering*. **196**. 66-75. 2006.

[6] B. Hassani. E. Hinton. A review of homogenization and topology optimization I - homogenization theory for media with periodic structure. *Computers and Structures*. **69**. 707-717. 1998.

[7] P.W. Chung. K.K. Tamma. R.R. Namburu. Asymptotic expansion homogenization for heterogeneous media: computational issues and applications. *Composites Part A*. **32**. 1291-1301. 2001

[8] O. Sigmund. Materials with prescribed constitutive parameters: An inverse homogenization problem. *International Journal of Solids and Structures*. **31**(17). 2313-2329. 1994.

[9] P.G. Coelho. L.D. Amiano. J.M. Guedes. H.C. Rodrigues. Scale-size effects analysis of optimal periodic material microstructures designed by the inverse homogenization method. *Computers and Structures*. Doi:10.1016/j.compstruc.2015.10.001. In Press.

[10] P.G. Coelho. S.J. Hollister. C.L. Flanagan. P.R. Fernandes. Bioresorbable scaffolds for bone tissue engineering: optimal design, fabrication, mechanical testing and scale-size effects analysis. *Med Eng Phys*. 37(3). 287-296. 2015.

[11] O. Sigmund. On the optimality of bone microstructure. P. Pedersen, M. Bendse eds. *IUTAM Symposium on Synthesis in Bio Solid Mechanics*. Kluwer. 221–234. 1999.

[12] R.T.L. Ferreira. H.C. Rodrigues. J.M. Guedes. J.A. Hernandes. Hierarchical optimization of laminated fiber reinforced composites. *Composite Structures*. **107**. 246-259. 2014.

[13] J.M. Guedes. N. Kikuchi. Preprocessing and postprocessing for materials based on the homogenization method with adaptive finite element method. *Comput Meth Appl Mech Eng*. **83**.143-198. 1990.

[14] T.I. Zohdi, P. Wriggers. *Introduction to computational micromechanics*. Springer. 2004.